Published Online First: January, 2024
https://doi.org/10.21123/bsj.2024.8834
P-ISSN: 2078-8665 - E-ISSN: 2411-7986
Baghdad Science Journal

Synthesis, Structural, Morphological Characterization, and Cytotoxicity Assays of Metal Complexes Decorated SiO_2 Nanoparticles Against Breast Cancer Cell Lines (MDA-MB-231)

***Alya'a J. Ahmed* [1], *Mahasin F. Alias*[2]**

[1]Ministry of Higher Education and Scientific Research,Baghdad, Iraq.
[2]Department of Chemistry, College of Science for Women, University of Baghdad, Baghdad, Iraq.
*Corresponding Author.

Received 01/04/2023, Revised 04/20/2023, Accepted 06/20/2023, Published Online First 20/01/2024

Abstract

This study examines the new synthesis of Pt (IV) and Au (III) Mannich base complexes derived from ciprofloxacin. The complexes were then used as precursors to prepare SiO2/PtO2 and SiO2/Au2O3 nanoparticles by depositing the synthesized complexes on porous silica nanoparticles. Elemental analysis, FT-IR, UV-vis, molar conductivity measurements, and melting point were used to characterize this ligand and its metal complexes. Elemental analysis data show that the general formula of the metal complexes formed is [M(L)2Cl2] nCl.H2O, where L = Mannich base ligand and M = Au(III) and Pt(IV), and n = 1,2 respectively with octahedral structure. The chemical structure and morphology of the metal oxide nanoparticles are investigated using FT-IR, XRD, AFM, TEM, and SEM. In the next step, the ligand and its complexes, SiO2/PtO2 and SiO2/Au2O3 nanoparticles were examined to investigate their toxicity (in vitro) as an anticancer agent to MDA-MB-231 cell lines by using different concentrations (50, 100, 200, and 400 µg /mL). Based on the results obtained from the cytotoxic activity, it can be concluded that the synthesized compounds are promising as new cancer candidates in the future, especially in high concentrations.

Keywords: Cytotoxicity assays, Ciprofloxacin, Metal oxides Nanoparticles, Mannich base complexes, Silica nanoparticles.

Introduction

The field of nanomedicine is a constantly evolving area of nanotechnology that has numerous applications in the biomedical field [1,2]. Nano therapeutics of the nanoparticle class have been shown to have a higher desired effect compared to conventional medications. This is due to surface functionalization, which can enhance the solubility, biocompatibility, and specific targeting capacity of nanoparticles. Metal and metal oxide nanoparticles can be synthesized and modified with a variety of chemical functional groups, allowing for a wide range of applications. By employing the necessary functionalization techniques, nanoparticles can be linked with biological molecules such as antibodies, nucleic acids, peptides, targeting ligands, DNA binding and even anticancer drugs [3-5]. Inorganic nanoparticles, such as mesoporous silica nanoparticles (MSN), have been extensively researched for their potential use in the delivery of drugs and other biomolecules, including proteins,

Published Online First: January, 2024
https://doi.org/10.21123/bsj.2024.8834
P-ISSN: 2078-8665 - E-ISSN: 2411-7986
Baghdad Science Journal

peptides, and nucleic acids. While antibiotics have traditionally been used to treat infectious diseases, the need for high in vivo drug dosages and the associated links to resistance have become a primary concern. As a result, there has been growing interest in the use of antimicrobial peptides (AMPs) as an alternative class of antimicrobials. Antibiotic delivery is particularly prone to proteolytic degradation at infection sites, which greatly impairs its activity. Additionally, direct delivery of antibiotics can lead to unwarranted toxic effects. However, nanotechnology can effectively address these issues by providing high loading capacity, site-directed delivery, and in some cases, triggered medication release. One promising approach is the use of drug delivery systems with a silica-gold core nanoshell, which offers numerous benefits over traditional dosage forms[6]. The use of Silica-Gold core nanoshells and PtNPs-based platforms for targeted drug delivery represents a promising area of research for the development of more effective cancer treatments. With further research and development, these technologies have the potential to revolutionize cancer treatment and improve patient outcomes [7,8]. Additionally, the potential for regulated transport of drugs may further reduce systemic exposure by controlling the release of drugs at the target site [9,10]. According to several research, using nanoparticles as part of synergistic therapy for the treatment of cancer not only enables cellular targeting but also lowers the risk of side effects, improves therapeutic effectiveness, and enhances the patient's long-term prognosis [11,12]. Thus, in this work we present the synthesis of Pt^{+4} and Au^{+3} complexes derivative from ciprofloxacin as precursors to prepare SiO_2/PtO_2 and SiO_2/Au_2O_3 nanoparticles by depositing the synthesized complexes on porous silica nanoparticles. The ligand and its complexes, SiO_2/PtO_2 and SiO_2/Au_2O_3 nanoparticles were examined to investigate their toxicity *(in vitro)* as an anticancer agent to MDA-MB-231 cell lines.

Materials and Methods

General

Ciprofloxacin (99.5%), 2-mercapto benzimidazole, formaldehyde, solvents, and metal chlorides (analytical grade) were obtained from Merck (Schnelldorf, Germany). Using an AA-6880 Shimadzu atomic absorption flame spectrophotometer (Shimadzu Corporation; Tokyo, Japan), the metal content was measured. A Bruker Avance 300 spectrometer (Bruker BioSpin GmbH, Rheinstetten, Germany) .To measure the ultraviolet-visible (UV-vi's) spectra in ethanol, a Shimadzu UV-1601 spectrophotometer (Shimadzu Company; Tokyo, Japan) was used. The FT-IR 8300 Shimadzu spectrophotometer (Shimadzu Corporation; Tokyo, Japan) was used to record the Fourier transform infrared (FTIR) spectra. Direct Probe captured mass spectra. The melting points in open glass capillaries were examined. Using EA-034. The myth, and the elemental analyses (C.H.N.S.) were obtained. Measurements of conductivity were performed using a Corning conductivity meter 220, and they were done in an ethanol solvent with a concentration of (10^{-3} M). Field emission scanning electron microscopy (FESEM) images were recorded using a Tescan MIRA3 LMU instrument (Tescan Orsay Holding; Brno-Kohoutovice, Czech Republic). FT-IR was recorded with a PerkinElmer BX spectrometer (4000−400 cm^{-1}) in KBr pellets. Whereas the powder XRD data were recorded on a diffractometer (X-ray tube target: CuKα (λ = 1.5406 nm). The AFM measurements were recorded by the instrument Veeco's Atomic Force Microscope and JEOL-(JEM) 12 30 transmission electron microscope. The surface area of the nanoparticles was evaluated using the Brunauer–Emmett–Teller (BET) method. Accurately weighted nanoparticles were degaussed at room temperature for 24 h to obtain 2 μmHg pressure. The surface area was determined via the multipoint nitrogen adsorption method (ASAP 2000, Micrometric, Norcross, GA, USA) Instrumentation.

Synthesis of mannich base ligand (7-(4-(((1H-benzo[d]imidazol-2-yl)thio)methyl)piperazin-1-yl)-1-cyclopropyl-6-fluoro-4-oxo-1,4-dihydroquinoline-3-carboxylic acid).

General procedure for the preparation of ligand (CPFX, 1.65 g 0.005 mol) and 2-mercaptobenzimidazole (0.75 g, 0.005 mmol) in EtOH (25 mL). A solution (CH_2O) was applied and

Published Online First: January, 2024
https://doi.org/10.21123/bsj.2024.8834
P-ISSN: 2078-8665 - E-ISSN: 2411-7986
Baghdad Science Journal

heated to reflux for 6 h and cooled at room temperature. The precipitate was filtered and recrystallized from (ethanol in water) to give the title compound[13], scheme.1.

Preparation of metal Complexes

The synthesis of metal complexes using a Mannich base ligand (L) and two different metal ions, Pt(IV) and Au(III). The procedure involves dissolving (0.493 g, 2 mmol) of the Mannich base ligand in 10 mL of absolute ethanol, followed by the addition of 5 ml of the metal ion (0.409g $H_2PtCl_6.6H_2O$ and 0.354 $HAuCl_4.6H_2O$ 1mmol). The resulting mixture is refluxed for 2 h, during which time the color of the solution changes. This change in color is likely due to the formation of the metal complex. After refluxing, the solvent is evaporated to yield a precipitate. This precipitate is then recrystallized from ethanol to purify the complex and finally dried to give the pure metal complex.

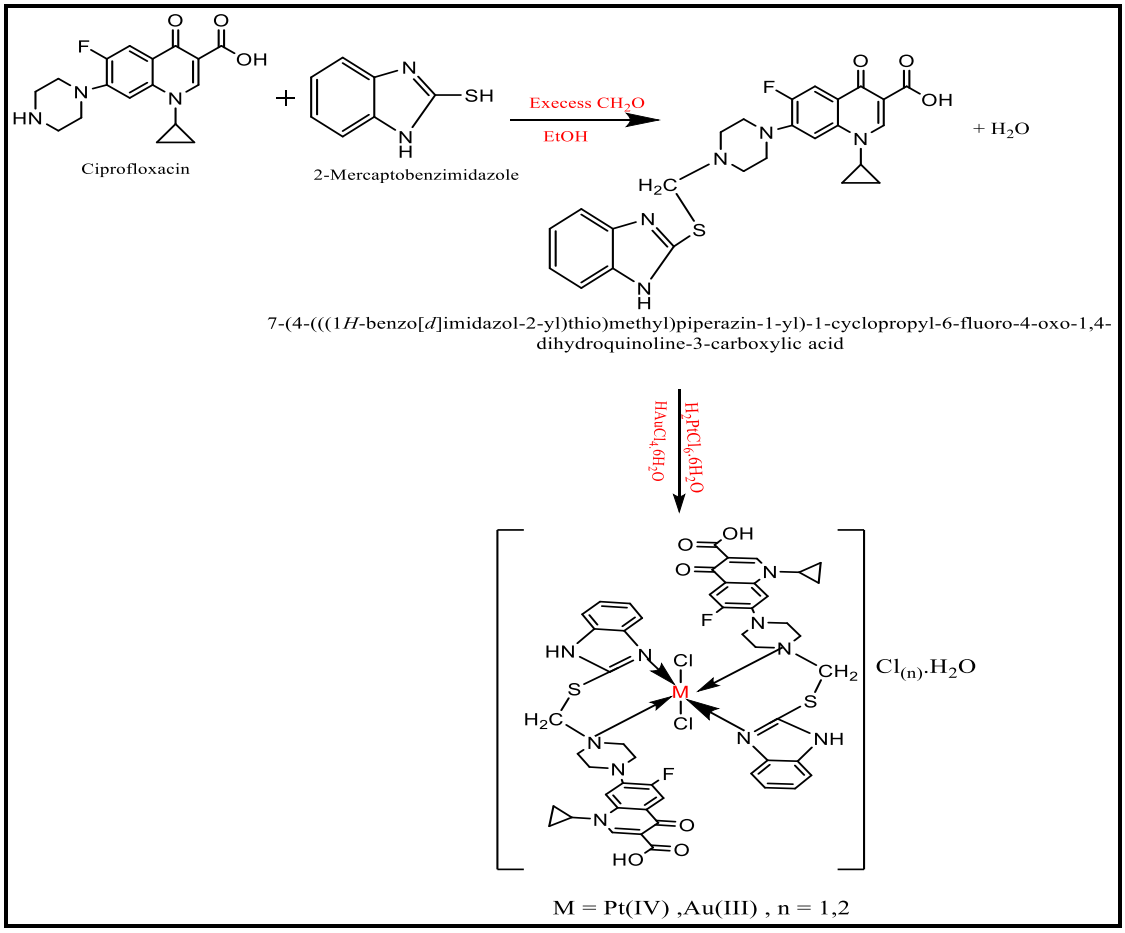

Scheme 1. Synthesis of ligand (L) and its complexes.

Synthesis of silica/metal oxide nanoparticles

The silica nanoparticles were subsequently functionalized by 0.03 g particles dissolved in ethanol followed by the addition of 0.05 g of Pt (IV) and Au(III) complex. The mixture was vigorously stirred at room temperature for 24 h to promote the covalent binding of Pt and Au onto the silica particles. The functionalized silica particles were centrifuged on R-24 refrigerated centrifuge (REMI) at 2000 rpm for 1 h and dried in a hot air oven at 60◦C. After then the precipitates were furnaces at 600◦C.

Biological activity

The cytotoxicity of ligand and its complex, SiO_2/PtO_2 and SiO_2/Au_2O_3 nanoparticles was studied against MDA-MB-231 cell lines by *in vitro* MTT cytotoxicity assay[14]. Cell lines were evaluated 24 h after being exposed to the compounds at

Published Online First: January, 2024
https://doi.org/10.21123/bsj.2024.8834
P-ISSN: 2078-8665 - E-ISSN: 2411-7986
Baghdad Science Journal

various concentrations. Results from the MTT testing utilizing a desiccator were shown for ligand and its complex, SiO_2/PtO_2 and SiO_2/Au_2O_3 nanoparticles. All the compounds produced were characterized using spectroscopy, analytical, and physical methods, as shown in Table.6. Various concentrations (400, 200, 100,50µg/ml) were compared to the untreated negative control culture medium.

Statistical analysis

Data were analyzed using IBM SPSS software version 91th ed. SAS. Inst. Inc. Cary. N.C. USA. The Statistical Analysis System- SAS (2018) program was used to detect the effect of different factors in study parameters. The least significant difference –LSD test (Analysis of Variation-ANOVA) was used to significantly compare between means in this study.

Results and discussion

Characterization of the ligand and their complexes

The data in Table 1 suggest that ligand (L) and its metal ion complexes are in agreement with calculated values. The suggested molecular structure is formulated and characterized by a subsequent spectral as well as magnetic moment.

Table1. Color, melting point, yield, and elemental composition of ligand and its metal complexes.

Comp.	suggested formula	Color	melting point ℃	yield %	M.Wt g.mol^{-1}	elemental analysis Found (cal.)				
						C	H	N	S	M
L	$C_{25}H_{24}FN_5O_3S$	Ligh Yellow	174-176	88.5	493.4	45.23 (45.63)	2.38 (2.78)	20.89 (21.2)	15.62 (16.2)	--- ---
PtL	$[PtL_2Cl_2]\ Cl_2.H_2O$	Dark Yellow	320d	74.14	1340	44.25 (44.28)	3.59 (3.67)	10.40 (10.4)	4.76 (4.84)	**14.5 (14.57)**
AuL	$[AuL_2Cl_2].Cl.H_2O$	Orange	253-255	75.04	1306	45.97 (46.04)	3.70 (3.78)	10.72 (10.8)	4.91 (4.99)	**15.81 (15.89)**

Spectral Analysis

The FT-IR spectrum of ligand (L) mannich base (2-mercaptobenzimidazole) derivative from ciprofloxacin Fig. 1 is concerning because there are several groups with overlapping regions, but a few of the bands are chosen to demonstrate the complex nature. Table 2 lists the principal IR bands of the free ligand and its metal complexes. The spectrum of ligand shows stretching frequency of ν (CH_2-N), ν (C=N), at (2964-2839), (1552), cm^{-1} respectively, the other bands appeared in 3531,1708,1627,1051,1361,1271,1137,738 cm^{-1} are assigned to stretching frequency of ν OH of COOH group, ν C=O, ν NCS, ν NCN, ν CNC, ν CSC, and ν CS respectively. The FTIR spectrum of the Au Complex Fig. 2 shows, the frequencies at 1707 cm^{-1} and 1627 cm^{-1}, respectively, are ascribed to the ν (C=O) of the carboxylic and carbonyl groups. In comparison to the free ligand, these vibration bands occur at the same frequencies (1708 cm^{-1} and 1627 cm^{-1}) [15]. These results showed that no carboxylic and carbonyl groups of oxygen atoms participated in the coordination of metal ions. In the Infrared spectra of complexes, the ν NH, bands did not change in intensity and position when comparing the same bands of the ligand, this proves the amine does not coordinate. The bands at 2964 2839 cm^{-1} which were attributed to the ν (CH_2-N) of the ligand mentioned previously were shifted to higher wave numbers in both complexes about 6-15 and 1-13 cm^{-1}, while the band in 1552 which to the ν (C=N) of the imidazole ring shifted to lower wave number in both complexes about 9-44 cm^{-1} as shown in Table 2 . This indicates that the ligand acts as a

Published Online First: January, 2024
https://doi.org/10.21123/bsj.2024.8834
P-ISSN: 2078-8665 - E-ISSN: 2411-7986
Baghdad Science Journal

neutral bidentate through the N atom of the Munich base and through the N atom of the imidazole ring. The weak absorption bands present at frequencies below 500 cm^{-1} are assigned to the coordination bonds ν (M-N) [16] between the metal ion and nitrogen atom of the Munich base derivative from ciprofloxacin. The complex spectra exhibited new weak bands at a frequency range 347-368 cm^{-1} assigned to stretching frequency of (M-Cl) [17] for pt(IV) and Au(III) complexes. In two complexes appeared bands varying between 3383-3487 cm^{-1} which refers to the stretching band of water incoordination.

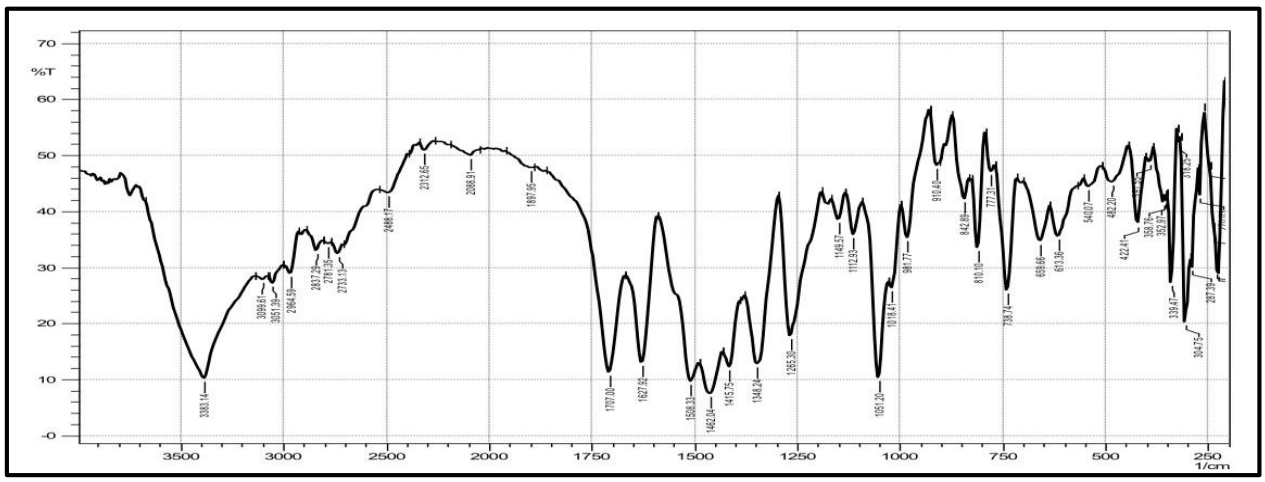

Figure 1. FTIR spectrum of ligand.

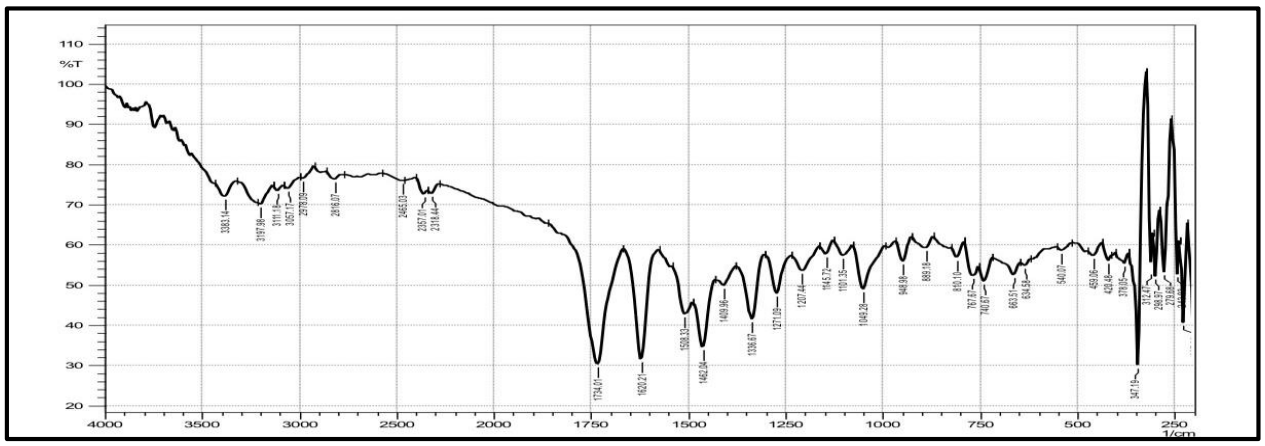

Figure 2. FTIR spectrum of Au complex.

Table 2. Selected FT-IR absorption bands of ligand and its metal complexes.

Comp.	ν COOH	ν C=O	νC-N ν N-C-N	ν N-H Imidazole Ring	νCH_2-N	ν C=N	νM-N	Others
L	1708	1627	1271 1107	3203	2964 2839	1552	----	----
PtL	1710	1629	1273 1107	3200	2972 2845	1543	480	ν (H_2O) = 3487 ν Pt-Cl = 368
AuL	1713	1620	1271 1101	3201	2978 2852	1508	459	ν (H_2O) = 3383 ν Au-Cl = 347

Published Online First: January, 2024
https://doi.org/10.21123/bsj.2024.8834
P-ISSN: 2078-8665 - E-ISSN: 2411-7986
Baghdad Science Journal

Electronic spectral

Electronic spectral studies of the ligand and both complexes were carried out in ethanol. The electronic spectrum of the Mannich base ligand shown in Table 3, Fig. 3 generally exhibited four main bands. The first and second absorption bands appeared at 30211, 32573, 35460 cm^{-1} due to interaligand (n → π*) transition of the carbonyl and -N=C- groups of imidazole in addition to the brazen ring. The third absorption band located at 40322 cm^{-1} attributed to (π → π*) electronic transition of the aromatic rings[18].

[PtL] Electronic spectrum of the prepared behavior dark yellow Pt (IV) complex Fig. 4 showed four bands at 98135,2777,32879 and 45248 cm^{-1} which are assigned to the transitions $^1A_1g \rightarrow$, ^3T_1g,$^1A_1g \rightarrow {}^1T_1g$,$^1A_1g \rightarrow {}^1T_2g$ and (L) → Pt (C.T) respectively [19]. The magnetic moment of the present complex is (0.0 B.M) of the present pit(IV) complex (d^6) configuration agrees with the octahedral configuration, this result indicates a diamagnetic. The conductivity measurement in ethanol showed that the complex was conducting, therefore the two (Cl^-) ions are located outside the coordination zone. From the analysis of data and spectroscopy techniques, and from all results, the octahedral prepared for this complex can be suggested.

[AuL] UV-vi's spectrum of orange Au(III) complex Fig. 5 showed two bands at 24570 and 35333 cm^{-1} assigned to $^3A_2g \rightarrow {}^3T_2g$, $^3A_2g \rightarrow {}^3T_1g$ transition respectively and other bands which appeared at 41152 cm^{-1} and 46296 cm^{-1} which could be due to the L→Au CT. The value of the Racah parameter B' has been calculated by fitting the ratio ν_2/ν_1 to the Tanabe-Sugano diagram for the octahedral d^8 system. The Dq/ B'=2.80; therefore, B' will be 842. The value of the constant field splitting Dq=2392.3 cm^{-1} and 10 Dq will be 23923 cm^{-1} which is in agreement with the octahedral environment reported [20]. So the third transition was calculated theoretically from the equation $15B\backslash= \nu_3+\nu_2-3\nu_1$, and found to be 51613 cm^{-1}, attributed to $^3A_2g \rightarrow {}^3T_1g$ (p) transition. The conductivity measurement for this complex shows to be ionic in nature. From the analysis of data and spectroscopy techniques, and from all results, the distorted octahedral prepared for this complex can be suggested.

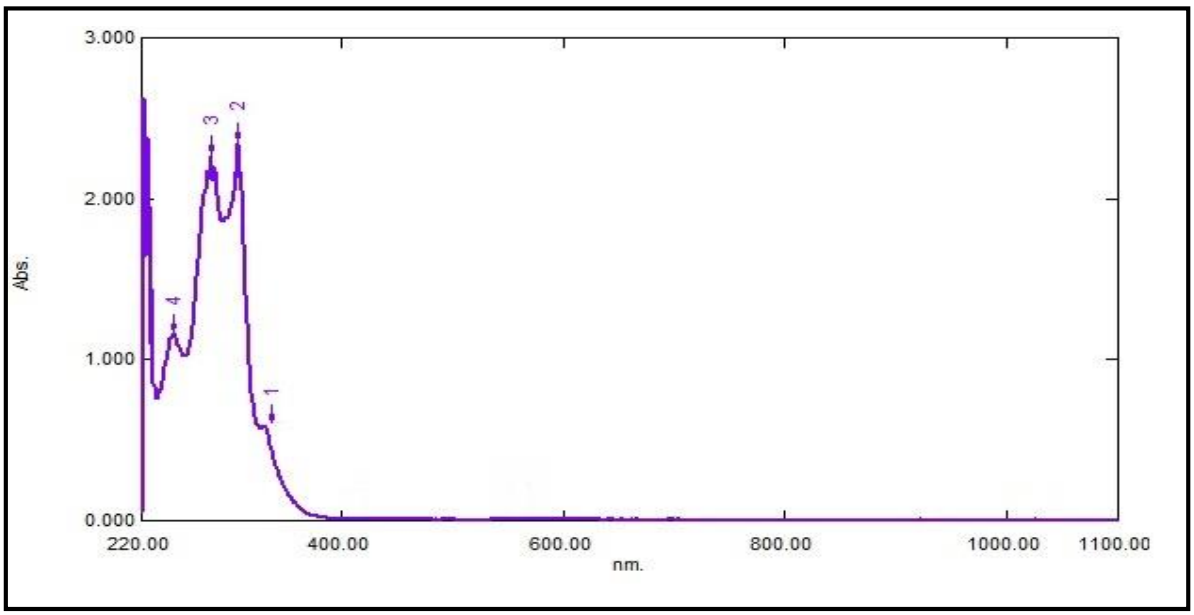

Figure 3. UV-VIS spectrum of L.

Published Online First: January, 2024
https://doi.org/10.21123/bsj.2024.8834
P-ISSN: 2078-8665 - E-ISSN: 2411-7986
Baghdad Science Journal

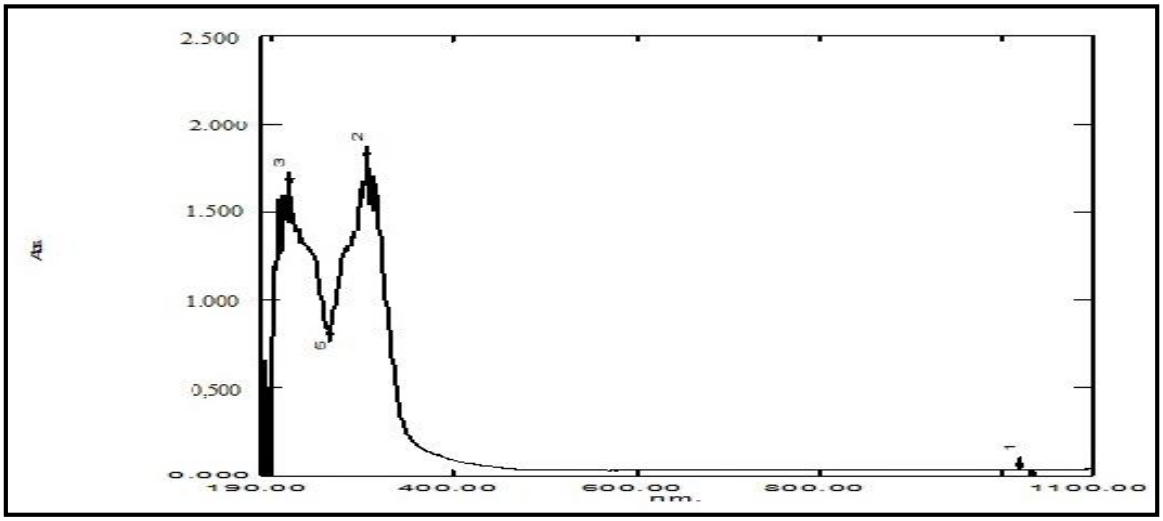

Figure 4. UV-VIS spectrum of Pt(IV) complex.

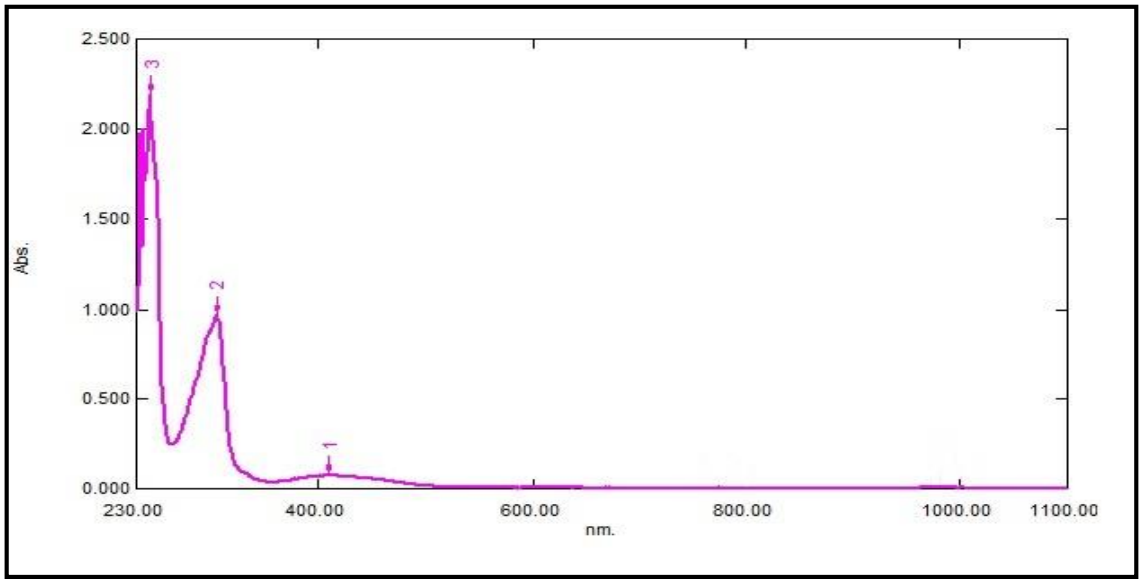

Figure 5. UV-VIS spectrum of Au(III) complex.

Table 3. Electronic transitions, conductivity, and suggested geometry of metal complexes.

Mass Spectroscopy

Comp.	Absorption Cm^{-1}	Assignments	B'	15 B'	10Dq	μeff B.M	$\mu s Cm^{-1}$	Suggested Geometry
L	30211,32573,35460	$n \rightarrow \pi *$						
	40322	$\pi \rightarrow \pi *$	---		---	---	---	**---**
Pt(IV)	98135	$^1A_1g \rightarrow {}^3T_1g$	---	---	---	0.00	85	**Distorted Octahedral**
	2777	$^1A_1g \rightarrow {}^1T_1g$						
	23879	$^1A_1g \rightarrow {}^1T_2g$						
	45248	(L) → Pt C.T						
Au(III)	24570	$^3A_2g \rightarrow {}^3T_2g$	842	12630	23923	2.51	61	**Distorted Octahedral**
	35333	$^3A_2g \rightarrow {}^3T_1g$						
	51613 (cal.)	$^3A_2g \rightarrow {}^3T_1g(p)$						
	41152	(L) → Au C.T						

Published Online First: January, 2024
https://doi.org/10.21123/bsj.2024.8834
P-ISSN: 2078-8665 - E-ISSN: 2411-7986
Baghdad Science Journal

The mass spectrum is a technique used to calculate the molecular weight of the prepared compounds and determine the fragmentation that belongs to the compounds under study. The mass spectrum of the prepared ligand Fig. 6 was consistent with the proposed structural formula $C_{25}H_{24}FN_5O_3S$. The bands were recorded for the ligand in their spectrum, one of them was related to the molecular ion and observed at 494.4 m/z for ligand. Additional distinct peaks revealed in the mass spectra for each ligand were resulting from the successive fragmentation.

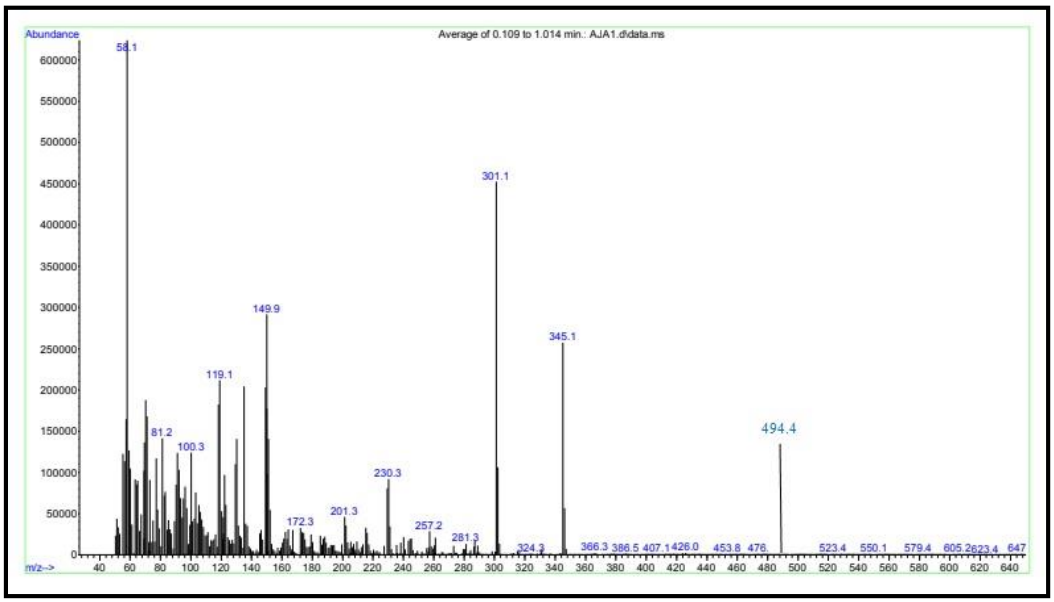

Figure 6. Mass spectrum of Ligand.

X-ray diffraction (XRD) pattern

In this study, XRD data was utilized to not only confirm the formation of different phases but also to calculate the particle size of each specimen. By analyzing the main peaks of each sample, the Debye- Scherrer equation was employed to determine the average particle size [21]:

$$D=k\lambda/\beta\cos\theta$$

Where D=crystallite site, k=shape factor =0.9, θ = diffraction angle at maximum peak intensity. β=full width at half maximum of diffraction angle in radians. λ= x-ray wavelength.

The X-ray diffraction analysis of the Au complex revealed interesting peaks that were compared to the standard d-values. The graph in Fig. 7 displays the index 2θ values for each peak, and it can be observed that there is good agreement between the 2 θ and d numbers. The diffraction peaks at 2θ values of 24.30, 27.733, 31.266, and 39.768 ° was identified as (101), (111), (002), and (211), respectively, in accordance with the Joint Committee on Powder Diffraction Standards requirements (JCPDS no. 04-0784) [22]. Table 4 presents the X-ray diffraction data for the Au complex, indicating the powder's moderate crystallinity.

Meanwhile, Fig. 8 displays the X-ray diffraction of a synthetic Pt complex, which exhibited distinct peaks at 2θ values of 11.7287, 13.845, 16.666, 17.713, 19.029, 24.587, 27.845 °. The metallic platinum-induced XRD patterns were compared to those of the JCPDS PDF card no. 04-0802 standard card[23], which showed similarities with the (111), (200), and (220) planes, respect. Based on the highest distinguishable peaks, the Au(III) and platinum(IV) complex grain sizes were estimated to be within 42 and 28.81 nm respectively.

Published Online First: January, 2024
https://doi.org/10.21123/bsj.2024.8834
P-ISSN: 2078-8665 - E-ISSN: 2411-7986
Baghdad Science Journal

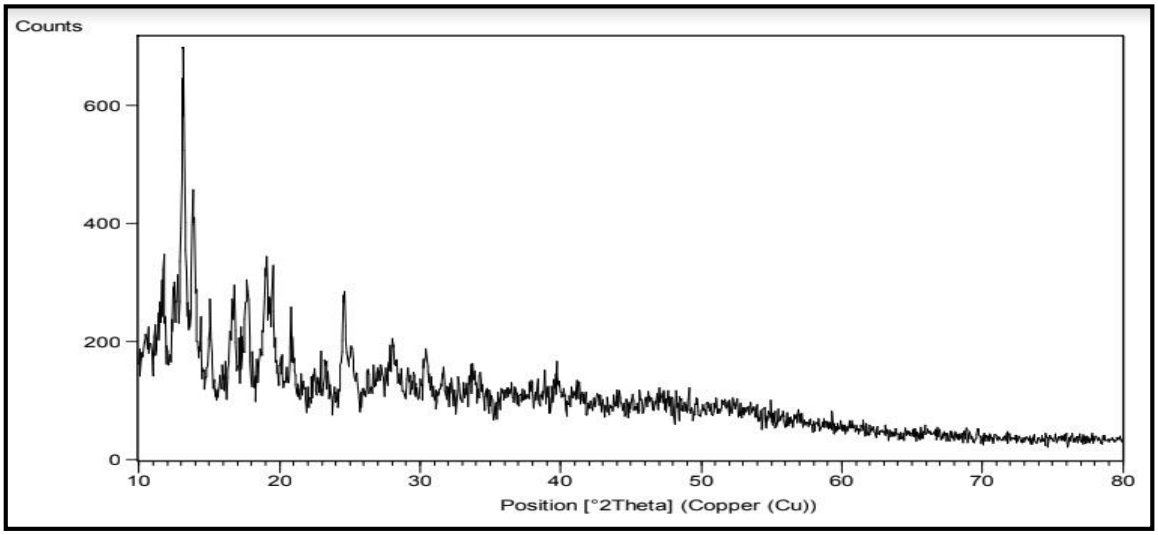

Figure 7.X-ray diffraction of Au complex.

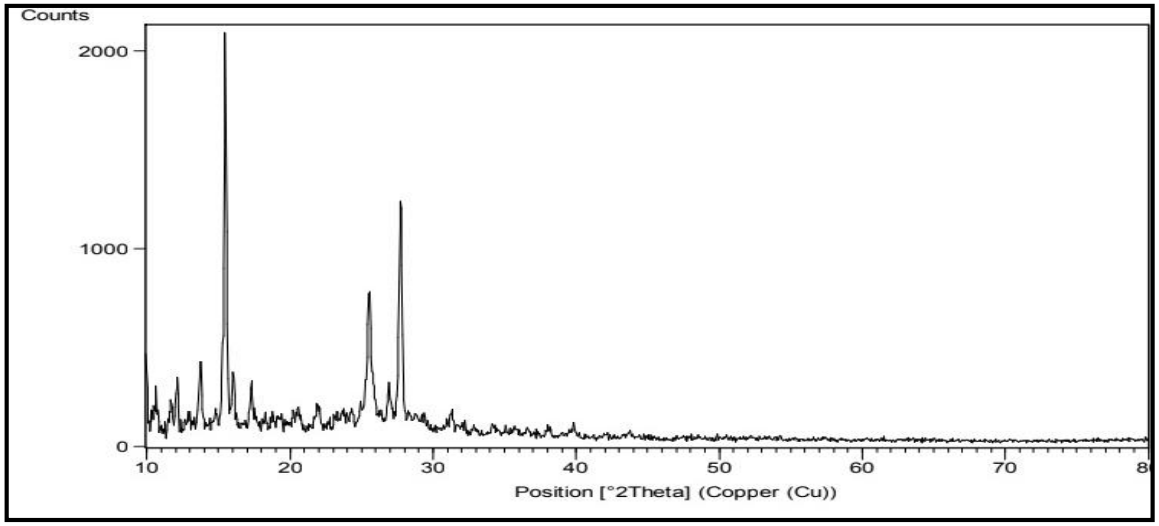

Figure 8.X-ray diffraction of pt complex.

Table 4. X-ray diffraction data of complexes

NO.	Complexes	2θ	FWHM	D-spacing (A)	Grain size (nm)
1	AuL	15.48	0.196	100	**42**
2	PtL	13.13	0.29	100	**28.81**

Characterization of SiO_2/ metal oxide nanoparticles

FT-IR spectra

The FT-IR spectrum of SiO_2 nanoparticles showed peaks appeared at around 3442 cm^{-1} and 1620 cm^{-1} which were attributed to molecular water and –OH bonding vibrations respectively [24]. Peaks that appeared at nearly 1105 cm^{-1} are attributed of stretching and out-of-plane vibrations of Si-O-Si bonds [25]. The band at 796.5 cm^{-1} is due to vibrations of SiO_4. The band that appeared at 474cm^{-1} is due to the out-of-plane deformation of Si-O [26]. In the spectrum of the SiO_2/PtO_2 and SiO_2/Au_2O_3, Fig. 9 and 10, the intensity of Si—O—Si and Si—OH peaks has been reduced significantly. This indicates the presence of PtO_2 and Au_2O_3 in silica particles. The weak absorption bands that appeared below 500 cm^{-1} are assigned to the coordination bonds of ν (Pt-O) and ν (Au-O) [27] .

Published Online First: January, 2024
https://doi.org/10.21123/bsj.2024.8834
P-ISSN: 2078-8665 - E-ISSN: 2411-7986
Baghdad Science Journal

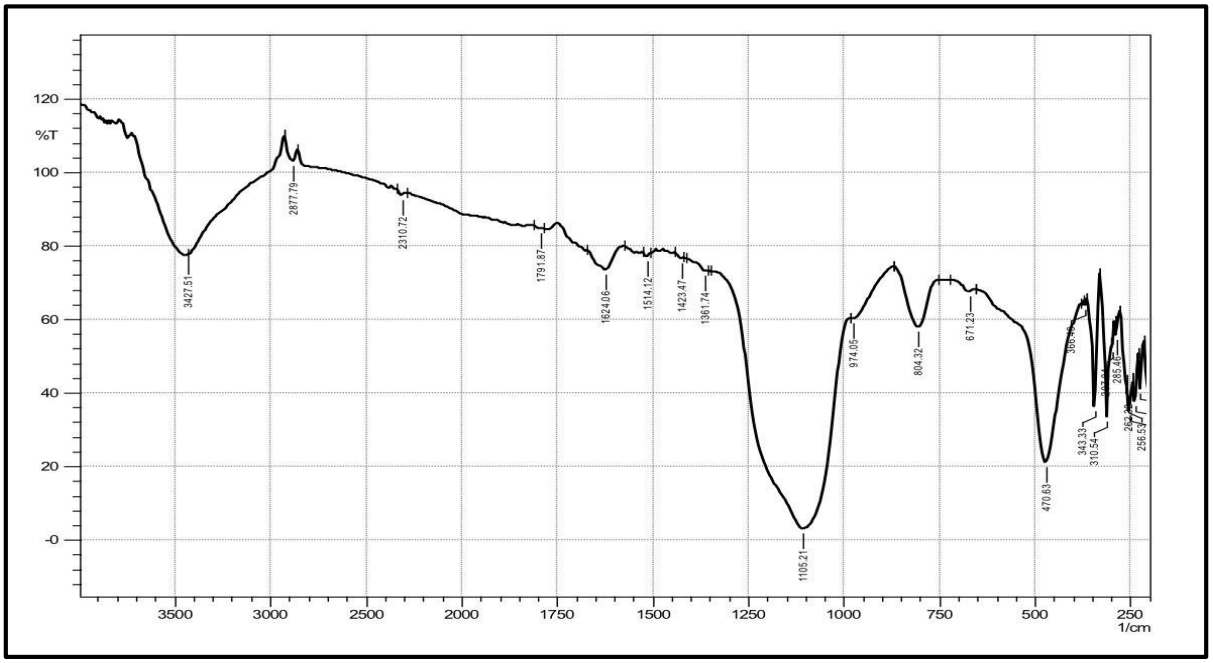

Figure 9.FTIR spectrum of SiO_2/PtO_2 nanoparticles.

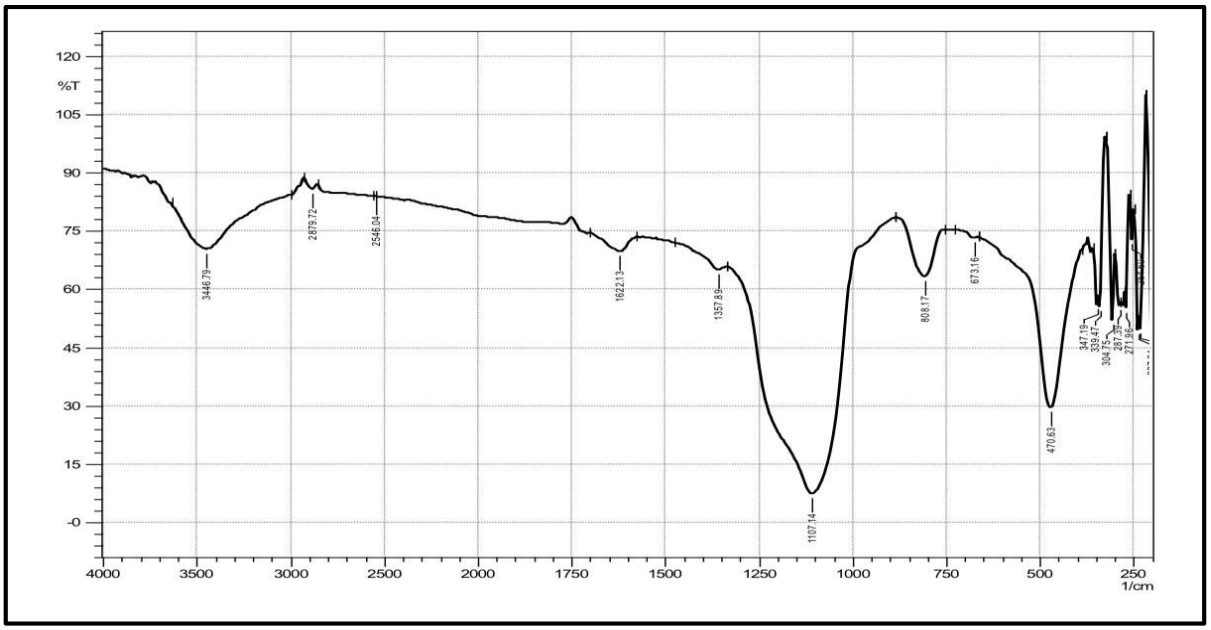

Figure10. FTIR spectrum of SiO_2/Au_2O_3 nanoparticles.

X-ray diffraction (XRD) pattern

Based on the information provided, Fig. 11a shows the X-ray spectrum of SiO_2 nanoparticles, which due to their amorphous nature, only show a broad band centered at 22°, which is typical for amorphous SiO_2. No distinguishable peaks in the diffraction pattern can be seen for them, except for that one. The results show no impurity peak for SiO_2 when compared to the JCPDS Card No. 850335 for SiO_2 [28]. In contrast, Fig 11b displays synthetic SiO_2/Au_2O_3 nanoparticles that are polycrystalline, with their respective crystal planes indexed as (400), (311), (202), (640), and (422) at 2θ = 24°, 2 = 39.77°, 2θ = 46.25°, 55.13°, and 67.49°, and the measured peaks and their angles are in good agreement with the Au_2O_3 nanoparticles X-ray spectra (JCPDS: 43-1039)[29]. Fig. 11c shows the XRD pattern of the distinctive peaks of the orthorhombic PtO_2 structure (JCPDS Card No. 75-1059) [30].

Published Online First: January, 2024
https://doi.org/10.21123/bsj.2024.8834
P-ISSN: 2078-8665 - E-ISSN: 2411-7986
Baghdad Science Journal

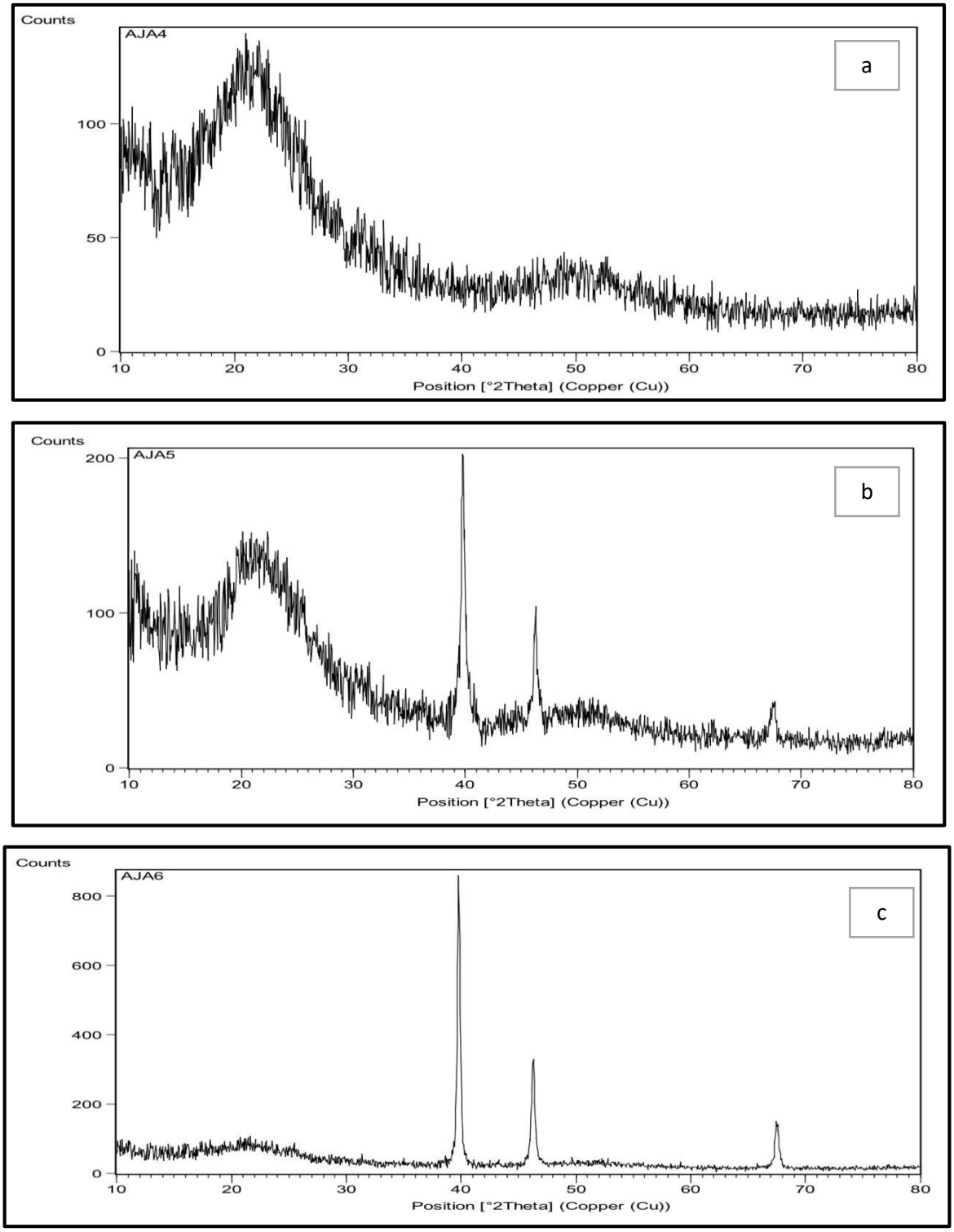

Figure 11. X-ray diffraction spectrum of (a) SiO_2 nanoparticles, (b) SiO_2/ Au_2O_3nanoparticales and (c) SiO_2/ PtO_2nanoparticales.

Morphological analysis

Transmission electron microscopy (TEM)

Nanoparticle size and shape are revealed via transmission electron microscopy (TEM). Figs. 12 and 13 demonstrate smaller agglomerated nanoparticles with spherical forms that are about in the range of 30 nm to 40 nm, for SiO_2/PtO_2 and SiO_2/Au_2O_3 nanoparticles respectively. Since metal

Published Online First: January, 2024
https://doi.org/10.21123/bsj.2024.8834
P-ISSN: 2078-8665 - E-ISSN: 2411-7986
Baghdad Science Journal

nanoparticles tend to agglomerate, the emergence of agglomerated nanoparticles is caused by aging and the absence of an anti- agglomeration factor in the colloidal aqueous solution.

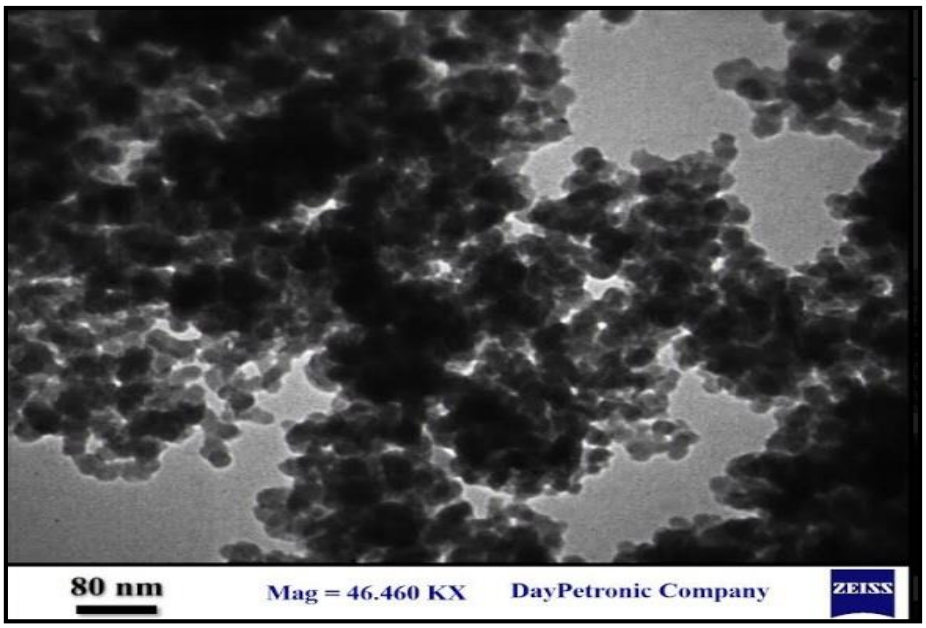

Figure12.TEM image of SiO_2/ PtO_2nanoparticales.

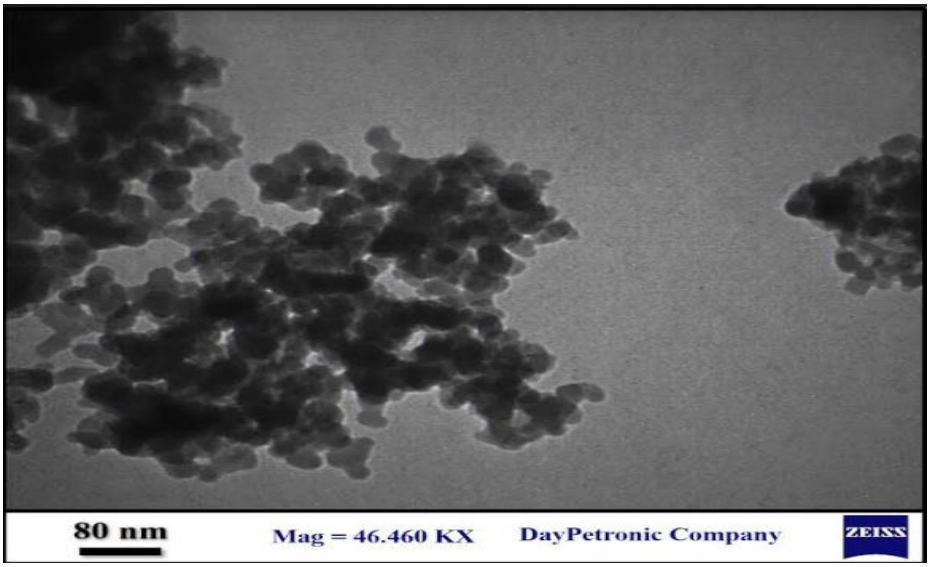

Figure13.TEM image of SiO_2/ Au_2O_3nanoparticales.

Scanning electron microscopy (SEM)

Figs. 14 and 15, show the morphology and size distribution of SiO_2/PtO_2 and SiO_2/Au_2O_3 nanoparticles, respectively. Nanoparticle surfaces have good crystallinity and are smooth. On the basis of random calculations, the average particle size and distribution for SiO_2/PtO_2 and SiO_2/Au_2O_3 nanoparticles are approximately 26 nm and 29 nm, respectively.

Published Online First: January, 2024
https://doi.org/10.21123/bsj.2024.8834
P-ISSN: 2078-8665 - E-ISSN: 2411-7986
Baghdad Science Journal

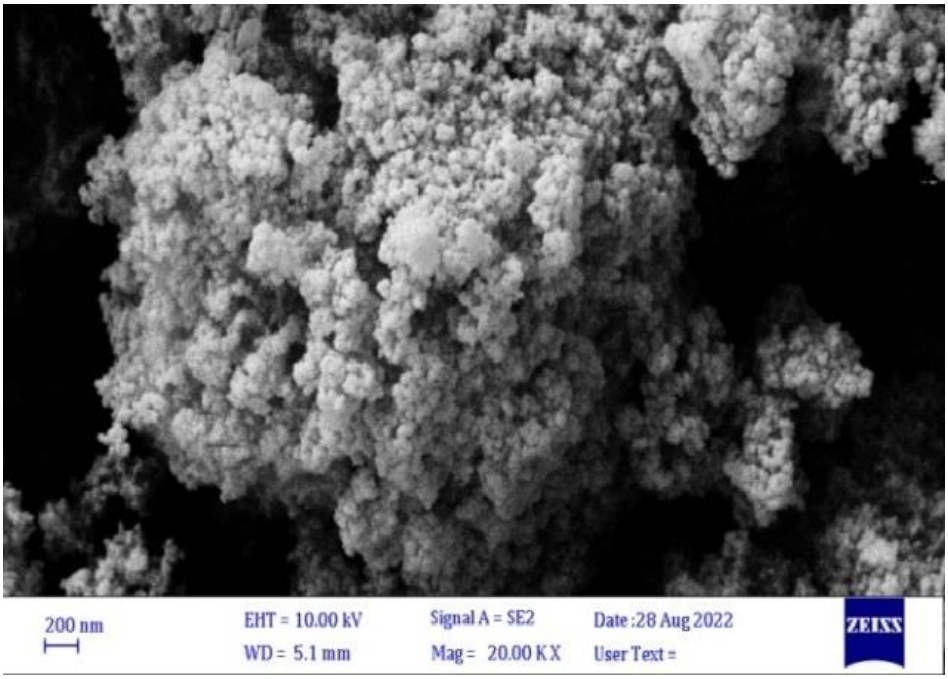

Figure14. SEM image of SiO_2/ PtO_2nanoparticales.

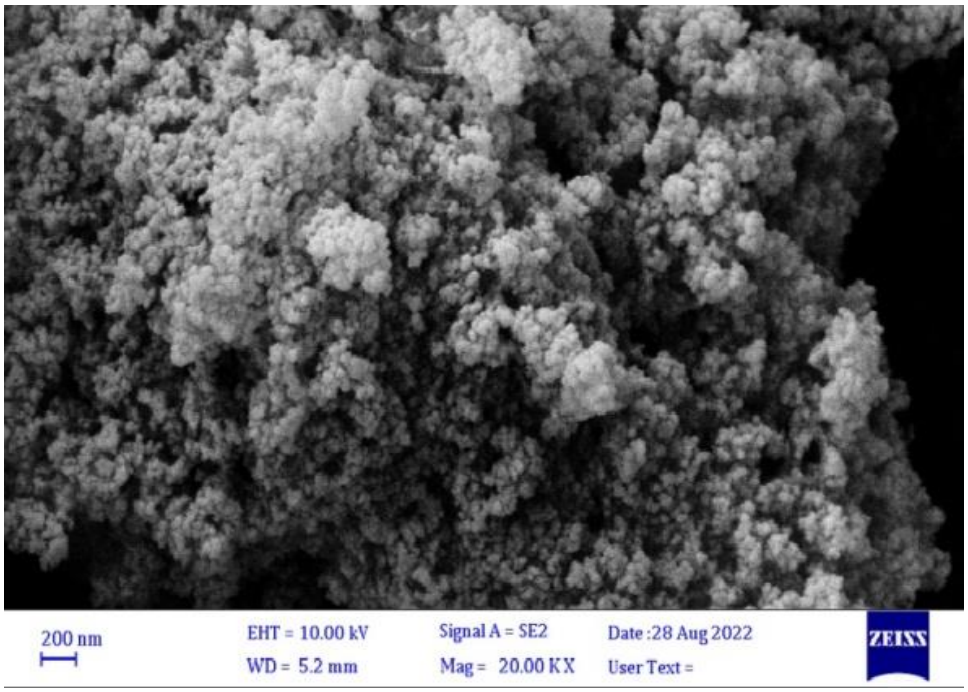

Figure15. TEM image of SiO_2/ Au_2O_3nanoparticales.

Atomic force microscopy (AFM)

The surface morphology and roughness of the produced nanoparticles have been characterized using the AFM. Fig. 16 and 17 display the three- and two-dimensional AFM images of SiO_2/PtO_2 and SiO_2/Au_2O_3 nanoparticles, respectively. According to the Figures, the obtained particle size distribution results for SiO_2/PtO_2 and SiO_2/Au_2O_3 nanoparticles are in the range of 5–17 nm and 3–18 nm, respectively. The average diameter of SiO_2/PtO_2 nanoparticles was 9.19 nm, and that of SiO_2/Au_2O_3 nanoparticles was 10.85 nm. This result demonstrates that these produced materials have nanoscale particles. The photos additionally display the SiO_2/PtO_2 and SiO_2/Au_2O_3 nanoparticles true

Published Online First: January, 2024
https://doi.org/10.21123/bsj.2024.8834
P-ISSN: 2078-8665 - E-ISSN: 2411-7986
Baghdad Science Journal

surface organization, which is characterized by the remarkable regularity of the surface objects.

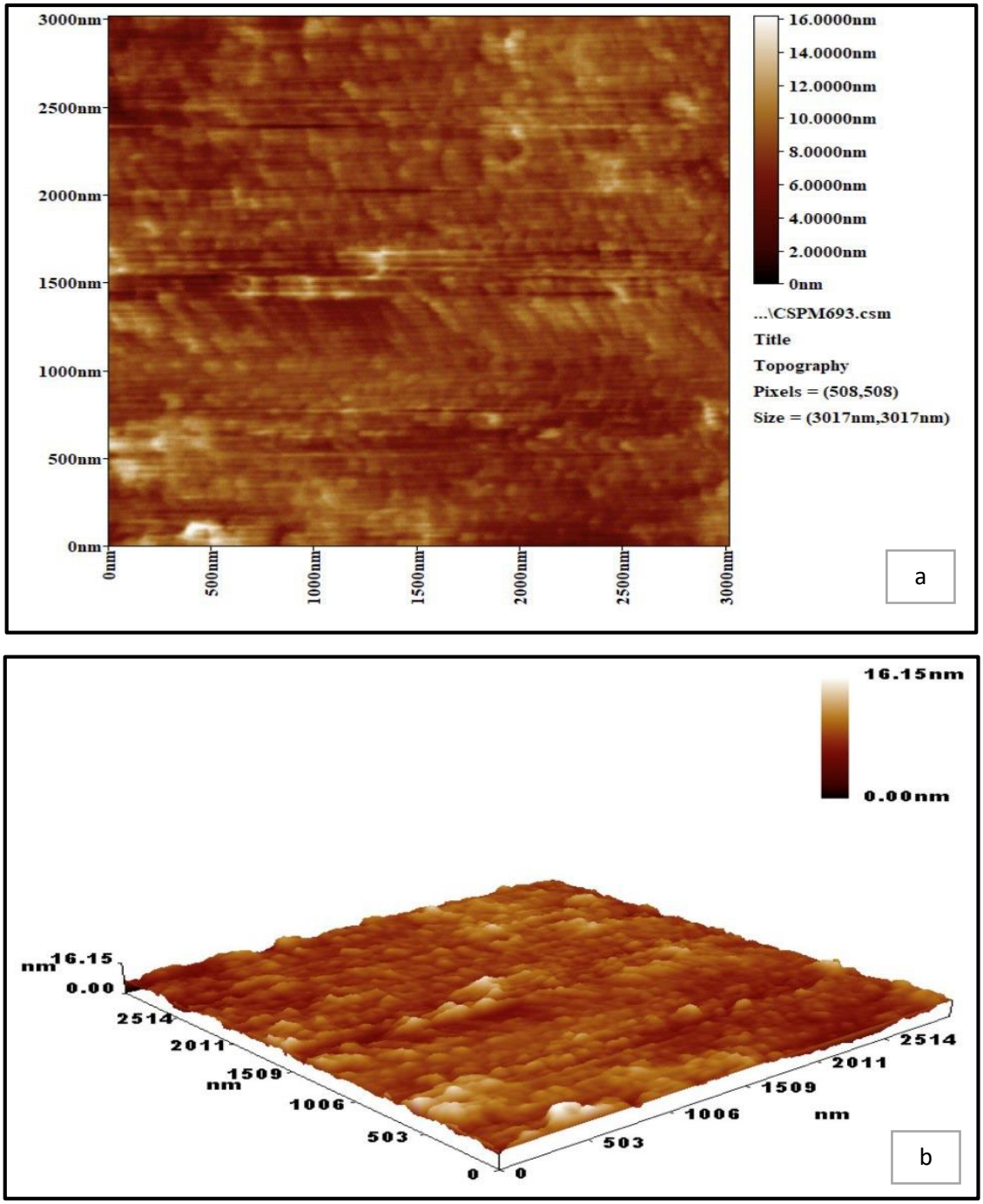

Figure 16. AFM image of SiO_2/ PtO_2 nanoparticles (a: two dimensional, b: three dimensional)

Published Online First: January, 2024
https://doi.org/10.21123/bsj.2024.8834
P-ISSN: 2078-8665 - E-ISSN: 2411-7986
Baghdad Science Journal

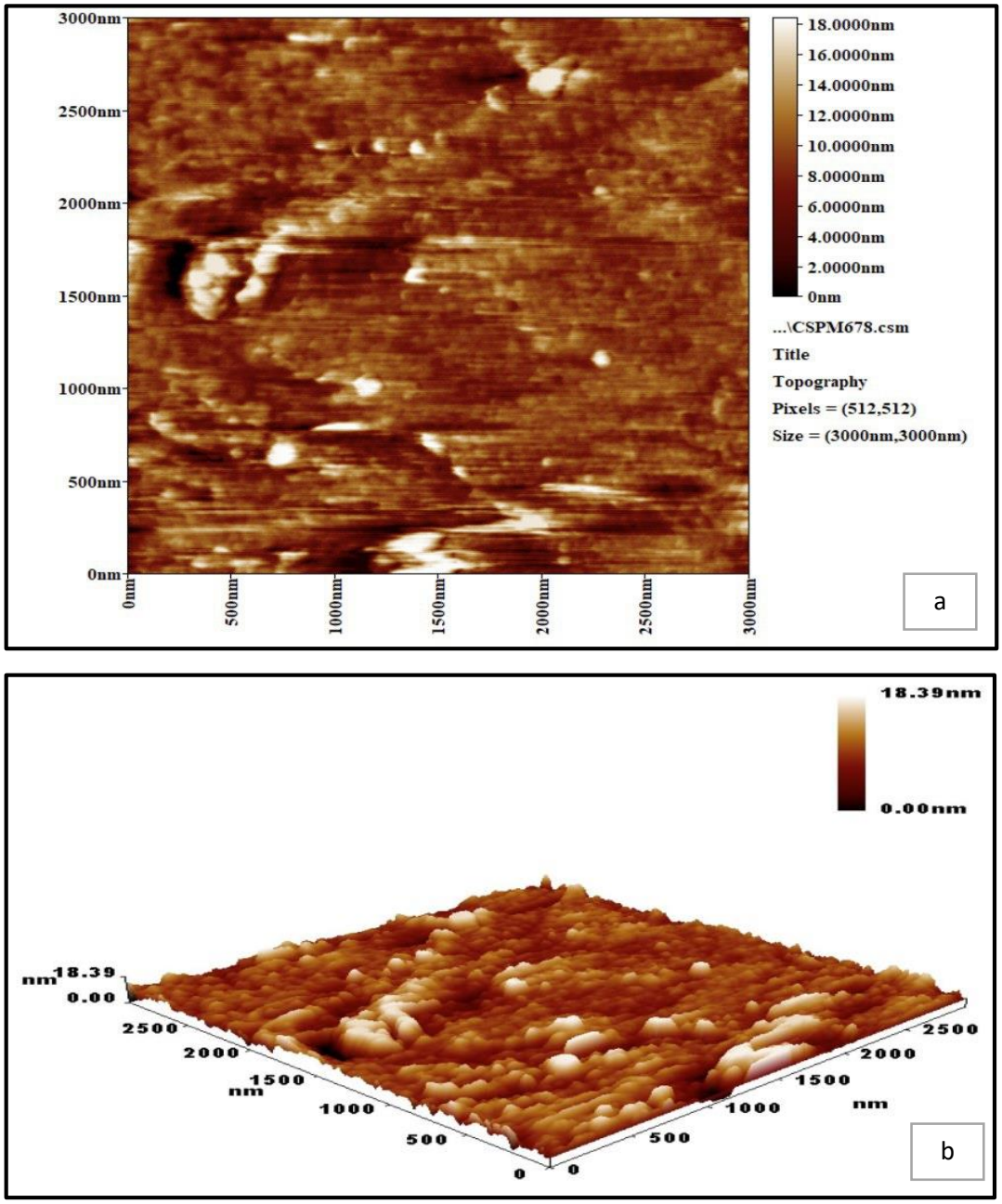

Figure 17. AFM image of SiO_2/ Au_2O_3 nanoparticles (a: two dimensional, b: three dimensional).

BET Surface Area Determination

The surface area and pore structure of the SiO_2/PtO_2 and SiO_2/Au_2O_3 nanoparticles were calculated using the nitrogen isothermal adsorption method depicted in Figs. 18 and 19. SiO_2/PtO_2 and SiO_2/Au_2O_3 nanoparticles isotherm profiles both displayed a modest hysteresis loop that might be categorized as type IV. Table 5 provides information about SiO_2/PtO_2 and SiO_2/Au_2O_3 nanoparticles, surface area, average pore diameter, and total pore volume. It is believed that the SiO_2/Au_2O_3 nanoparticles have high surface energy is what causes nanoparticle aggregation or the formation of larger nanoparticles. The SBET of SiO_2/PtO_2 and SiO_2/Au_2O_3 nanoparticles was calculated using the BET method from nitrogen adsorption/desorption measurements. The nitrogen adsorption isotherms at P/PO = 0.9 were used to calculate the BET surface area and pore volume. The Barrett-Joyner-Halenda (BJH) method was used to measure the size and volume of the pores, as shown in Table 5.

Published Online First: January, 2024
https://doi.org/10.21123/bsj.2024.8834
P-ISSN: 2078-8665 - E-ISSN: 2411-7986
Baghdad Science Journal

Table 5. Surface area and pore size distribution (PZD) of metal complexes by the N_2 adsorption

Comp.	SBET ($m^2.g^{-1}$)	Pore Volume ($Cm^3.g^{-1}$)	Average pore Diameter (nm)
SiO_2/PtO_2	70.21	0.85	48.66
SiO_2/Au_2O_3	188.22	1.96	41.82

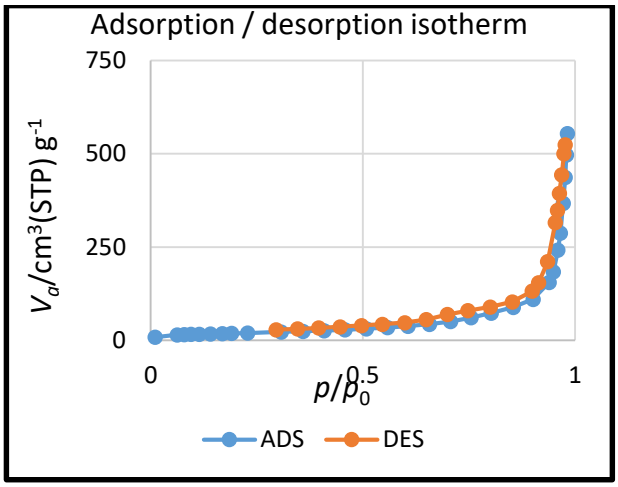

Figure 18. N_2 adsorbed isotherms of SiO_2/PtO_2

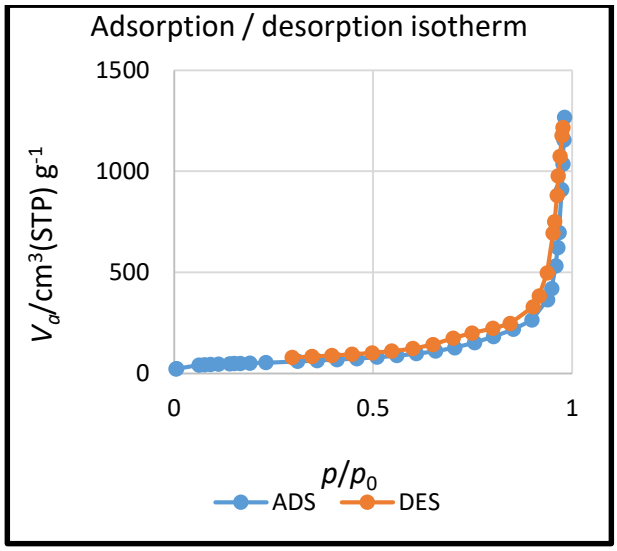

Figure 19. N_2 adsorbed isotherms of SiO_2/Au_2O_3.

Cytotoxic activity

The against-cancer impact we tested the cytotoxic activity of synthetic free ligand and its complex, SiO_2/PtO_2 and SiO_2/Au_2O_3 nanoparticles against MDA-MB-231 cell lines using the MTT assay after incubating the samples for 24 hours at 37°C and using doses of 50, 100, 200, and 400 µg /mL. The chosen compounds inhibited the MDA-MB-231 cell line growth in a variety of ways, and Table 6 comparisons of the percent inhibition of cell growth to the control provided determines the amount of the harmful effect. According to the cytotoxicity results, all tested compounds showed strong cytotoxicity against MDA-MB-231 cancer cells. The gold (III) complex showed the highest cytotoxicity effect with an LSD value of 9.53, followed by the platinum (IV) complex with an LSD value of 8.13, The ligand showed the less cytotoxicity effect with a value of 7.16. As the concentration of the compounds increased, cell viability decreased for MDA-MB-231 cancer cell lines. This is demonstrated in Fig. 20. The SiO_2/Au_2O_3 inhibited tumor cell death with an 87% cytotoxic efficacy. While MDA-MB-231 cell lines were suppressed by SiO_2/PtO_2 to an extent of (82%) at a dose of 400 µg /mL. This finding demonstrated that SiO_2/Au_2O_3 nanoparticles significant cytotoxic activity was caused by an increase in an Au_2O_3 surface area following homogeneous deposition on porous SiO_2. These results suggest that these compounds have potential as anticancer agents and warrant further investigation at a concentration of 400µg /ml.

Published Online First: January, 2024
https://doi.org/10.21123/bsj.2024.8834
P-ISSN: 2078-8665 - E-ISSN: 2411-7986
Baghdad Science Journal

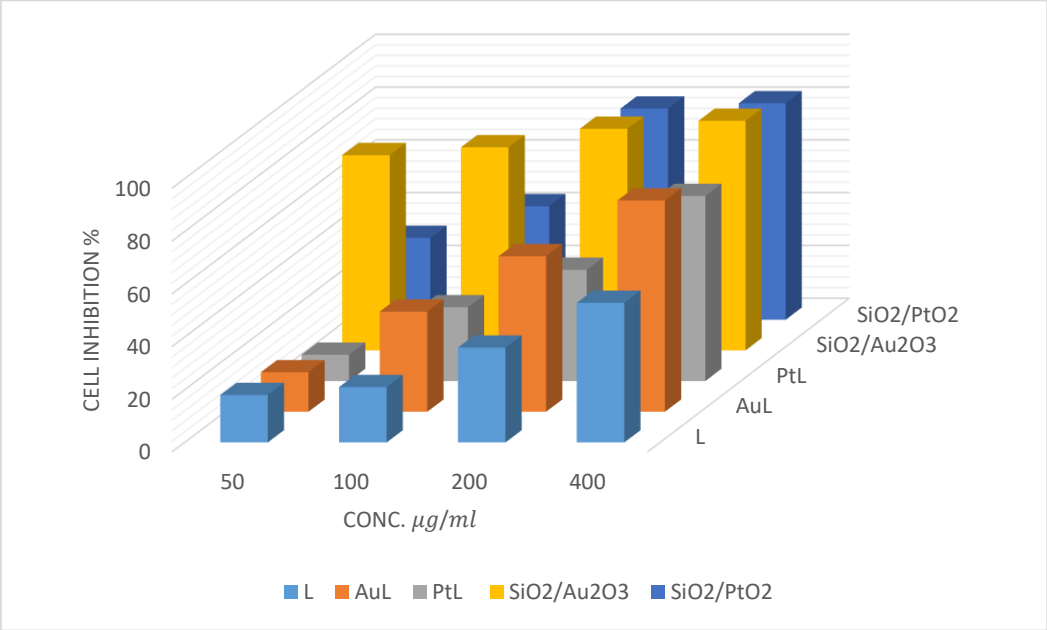

Figure 20. The percentage inhibition in 400, 200, 100, 50 µg/ml after exposure to ligand and its complex, SiO_2/PtO_2 and SiO_2/Au_2O_3 at 24 hrs.

Table 6. Evaluation of cytotoxicity of ligand, metal complex, SiO_2/PtO_2 and SiO_2/Au_2O_3 nanoparticles against MDA-MB-231 cell lines after incubation (24 hr) at (37 ◦C).

Comp.	%Cell Inhibition				LSD value
	Conch. $\mu g/ml$				
	400	200	100	50	
L	53.0 D a	36.0 C b	21.0 D c	18.0 A c	**7.16 ***
AuL	80.1 a	59.0 A b	38.0 A c	15.0 AB d	**9.53 ***
PtL	70.2 BC a	42.2 BC b	28.0 BC c	10.0 BC d	**8.13 ***
SiO_2/Au_2O_3	87 a	84 a	77 A b	74 A b	**8.91 ***
SiO_2/PtO_2	82 a	80 a	43 B b	31 B c	**8.57 ***

Means with different big letters in the same column and small letters in the same row are significantly different, * (P≤0.05).

Conclusion

The new Munich base ligand and its complex, SiO_2/PtO_2 and SiO_2/Au_2O_3 nanoparticles have been synthesized, deposited on porous SiO_2, and characterized the structure for the ligand and its complexes, the analysis and spectroscopy technique also morphological were determined using FT-IR, XRD, AFM, TEM, and SEM. It can be concluded from biological activity that ligand and its complex, SiO_2/PtO_2 and SiO_2/Au_2O_3 nanoparticles have good cytotoxic properties and selectivity against MDA-MB-231 cell lines. Cell viability and cytotoxicity assays were performed on the nanoparticles using MDA-MB-231 cell lines. It was discovered that SiO_2 plays a crucial role in dispersing Au_2O_3 nanoparticles across a large portion of its surface area and in preventing metal oxide nanoparticle aggregation.

Published Online First: January, 2024
https://doi.org/10.21123/bsj.2024.8834
P-ISSN: 2078-8665 - E-ISSN: 2411-7986
Baghdad Science Journal

Acknowledgment

We thank the University of Baghdad for technical support.

Author's Declaration

- Conflicts of Interest: None.
- We hereby confirm that all the Figures and Tables in the manuscript are ours. Furthermore, any Figures and images, that are not ours, have been included with the necessary permission for re-publication, which is attached to the manuscript.
- Authors sign on ethical consideration's approval.
- Ethical Clearance: The project was approved by the local ethical committee in Ministry of Higher Education and Scientific Research.

Author's Contribution

A.J.A., role Conception, design, acquisition of data. M F. A., role analysis, interpretation, drafting the MS, revision and proofreading.

References

1. Asharani P V, Xinyi N G, Hande M P, Valiyaveettil S. DNA damage and p53-mediated growth arrest in human cells treated with platinum nanoparticles. Nanomedicine. 2010; 5(1): 51-64. https://doi.org/10.2217/nnm .09 .85
2. Conde J, Doria G, Baptista P. Noble metal nanoparticle applications in cancer. J Drug Deliv.2012; (2012): 1-12. https://doi.org/10.1155/2012/751075.
3. Kang S J, Park S J, Mishig-Ochir T, Lee B J. Antimicrobial peptides: therapeutic potentials. Expert Rev Anti Infect There. 2014; 12 : 1477–1486.https://doi.org/10.1586/14787210.2014.976613.
4. Zhang C, Yan L, Wang X, Zhu S, Chen C, Gu Z, et al. Progress, challenges, and future of nanomedicine. Nano Today.2020 ;35: 101008. https://doi.org/10.1016/j.nantod.2020.101008.
5. Fahad A S, Thani M Z, Abdullah A M, Dhahir S A . Development of an Ecological-friendly Method for Ciprofloxacin Determination and Cloud Point Extraction in Pharmaceuticals using Fe (II)($FeSO_4$. $7H_2O$). IOP Conf Ser.: Mater Sci Eng. 2020; 871(1): 012028. https://doi.org/10.1088/1757-899X/871/1/012028.
6. Song T X, Silveira A P, Morais J AV, Sampaio M C, Muehlmann L A, Zhang J, et al. Recent advances in antimicrobial nano-drug delivery systems. Nanomaterials. 2022; 12(11): 1855. https://doi.org/10.3390/nano12111855.
7. Zeng X, Liu G, Tao W, Ma Y, Zhang X, He F, et al. A drug-self-gated mesoporous antitumor nanoplatform based on pH-sensitive dynamic covalent bond. Adv Funct Matter. 2017; 27(11): 1605985. https://doi.org/10.1002/adfm.201605985.
8. Majerník M, Jendželovský R, VargováJ, Jendželovská Z, Fedoročko P. Multifunctional Nanoplatforms as a Novel Effective Approach in Photodynamic Therapy and Chemotherapy, to Overcome Multidrug Resistance in Cancer. Pharmaceutics. 2022; 14(5): 1075. https://doi.org/10.3390/pharmaceutics14051075.
9. Liu S, Pan J, Liu J, Ma Y, Qiu F, Mei L, et al. Dynamically PEGylated and borate-coordination-polymer-coated polydopamine nanoparticles for synergistic tumor-targeted, chemo-photothermal combination therapy. Small. 2018; 14(13): 1703968. https://doi.org/10.1002/smell. 201703968.
10. Gao N, Nie J, Wang H, Xing C, Mei L, Xiong W, et al. A versatile platform based on black phosphorus nanosheets with enhanced stability for cancer synergistic therapy. J Biomed Nanotechnol. 2018; 14(11): 1883-1897. https://doi.org/10.1166/jbn. 2018. 2632.
11. Patel P, Nadar V M, Umapathy D, Manivannan S, Venkatesan R, Joseph Arokiyam V A, et al. Doxorubicin-Conjugated Platinum Theranostic Nanoparticles Induce Apoptosis via Inhibition of a Cell Survival (PI3K/AKT) Signaling Pathway in Human Breast Cancer Cells. ACSAppl. Nanometer. 2020; 4(1): 198–210. https://doi.org/10.1039/d0ra06708c.
12. Fu B, Dang M, Tao J, Li Y, Tang Y. Mesoporous Platinum Nanoparticle-Based Nanoplatforms for Combined Chemo-Photothermal Breast Cancer Therapy. J Colloid Interf. SCI. 2020; 570: 197–204. https://doi.org/10.1016/j. juicis. 2020. 02. 051e

Published Online First: January, 2024
https://doi.org/10.21123/bsj.2024.8834
P-ISSN: 2078-8665 - E-ISSN: 2411-7986
Baghdad Science Journal

13. Feng L S, Liu M L, Zhang S, Chai Y, Wang B, Zhang Y B, et al. . Synthesis and in vitro antimycobacterial activity of 8-OCH3 ciprofloxacin ethylene and ethylene isatin derivatives. EUR J Med Chem. 2011; 46(1): 341-348. https://doi.org/10.1016/j. ejmech. 2010. 11. 023.
14. Abdulameer J H, Alias M F. Heavy Metal Complexes of 1, 2, 3-Triazole derivative: Synthesis, Characterization, and Cytotoxicity Appraisal Against Breast Cancer Cell Lines (MDA-MB-231). Baghdad Sci J. 2022; 19 (6 Supplement). https://doi.org/10.21123/bsj.2022.7178
15. Sadiq A S, Khudhair Z T, Mahmood T A, Mahmood W A. Design, Synthesis, Theoretical Studies, and Effect of N-Mannich Base Ciprofloxacin Derivatives on the Activity of Some Transfer Enzymes. Indian J Heterocycl Chem. 2022; 32(04): 439-447. https://connectjournals.com/01951.2022.32.439.
16. Venkittapuram P R, Dhandapani M, Suyambulingam J, Subramanian C. Synthesis, characterization, thermal, theoretical and antimicrobial studies of Schiff base ligand and its Co (II) and Cu (II) complexes. J Serb Chem Soc. 2020 ;*85*(2): 215-225. https://doi.org/10.2298/JSC181128049V.
17. Shaalan N. Preparation, Spectroscopy, Biological Activities and Thermodynamic Studies of New Complexes of Some Metal Ions with 2-[5-(2-Hydroxy-Phenyl)-1, 3, 4-Thiadiazol-2-Ylimino] -Methyl-Naphthalen-1-Ol. Baghdad Sci J. 2022; 19(4): 0829-0829. https://doi.org/10.21123/bsj.2022.19.4.0829.
18. Al-Harazie A G, Gomaa E A, Zaky R R, Abd El-Hady M N . Spectroscopic Characterization, Cyclic Voltammetry, Biological Investigations, MOE, and Gaussian Calculations of VO (II), Cu (II), and CD (II) Heteroleptic Complexes. ACS omega. 2023; 8(15): 13605–13625. https://doi.org/10.1021/acsomega.2c07592.
19. Alosaimi E H. Spectroscopic Characterization, Thermogravimetry and Biological Studies of Ru (III), Pt (IV), Au (III) Complexes with Sulfamethoxazole Drug Ligand. Crystals. 2022; 12(3): 340. https://doi.org/10.3390/cryst12030340.
20. Mahdi Z. Alias M F. Synthesis, Characterization and Thermal Study of Some New Metal Ions Complexes with a New Azo 2-((2-(1H-Indol-2-yl) ethyl) diazinyl) -5-aminophenol. J Med Chem Sci. 2022; 6: 677-692. https://doi.org/10.26655/JMCHEMSCI.2023.1.15.
21. Baqer S R, Alsammarraie A MA, Alias M, Al-Halbosiy M M, Sadiq AS. In Vitro Cytotoxicity Study of Pt Nanoparticles Decorated TiO_2 Nanotube Array. cancer, 2020; 17(4): 1169-1176. https://doi.org/10.21123/bsj.2020.17.4.1169
22. Seku K, Yamala A K., Kancherla M, Kumar K K., BadathalaV. Synthesis of moxifloxacin–Au (III) and Ag (I) metal complexes and their biological activities J Anal SCI Technol. 2018; 9(1): 1-13. https://doi.org/10.1186/s40543-018-0147-z .
23. Al-Khodir F A, Abumelha H, Al-Warhi T, Al-Issa S A. New platinum (IV) and palladium (II) transition metal complexes of s-triazine derivative: synthesis, spectral, and anticancer agents studies. Biomed Res Int. 2019; (2019): 1-15. https://doi.org/10.1155/2019/9835745.
24. Shahbazi-Alavi H, Ebrahimi S M, Safaei-Ghomi J. CuO/ZnO@ N-GQDs@ NH_2 nanocomposite as superior catalyst for the synthesis of pyrimidine-triones. Nanochem Res .2021; 6(1): 10-17 . https://doi.org/10.22036/ncr.2021.01.002 .
25. Bodaghifard M A, Faraki Z, Asadbegi S. Effective fabrication of poly (anilin-formaldehyde)-supported hybrid nanomaterial and catalytic synthesis of dihydropyridines. Nanochem Res. 2019 ;4(2): 101-111. https://doi.org/10.22036/ncr.2019.02.001.
26. Suresh M, Kalaivani T. Synthesis and characterization of mesoporous SiO_2 nanoparticles for bio medical applications. Mater Sci Eng. 2022; 1219 (1): 012038. IOP Publishing. https://doi.org/10.1088/1757-899X/1219/1/012038.
27. Abdulridha MQ, Al-Hamdani AA, Mahmoud WA. Synthesis, Characterization and Thermal Study of Some New Metal Ions Complexes with a New Azo 2-((2-(1H-Indol-2-yl)ethyl)diazinyl)-5-aminophenol. J Med Chem Sci. 2023; 6 :121-131 . https://doi.org/10.26655/JMCHEMSCI.2023.1.15 .
28. Hussein E A, Kareem S H. Mesoporous silica nanoparticles as a system for ciprofloxacin drug delivery; kinetic of adsorption and releasing. Baghdad Sci J. 2021; 18(2): 357-365. https://doi.org/10.21123/bsj.2021.18.2.0357.
29. Ahmed D S, Mohammed M K. Studying the bactericidal ability and biocompatibility of gold and gold oxide nanoparticles decorating on multi-wall carbon nanotubes. Chem Pap. 2020; 74(11): 4033-4046. https://doi.org/10.1007/s11696-020-01223-0.
30. Sarno M, Ponticorvo E. Much enhanced electrocatalysis of Pt/PtO_2 and low platinum loading Pt/PtO_2-Fe_3O_4 dumbbell nanoparticles. Int J Hydrog Energy. 2017; 42(37): 23631-23638. https://doi.org/10.1016/j.ijhydene.2017.03.017 .

Published Online First: January, 2024
https://doi.org/10.21123/bsj.2024.8834
P-ISSN: 2078-8665 - E-ISSN: 2411-7986
Baghdad Science Journal

تحضير ، التوصيف البنيوي و المورفولوجي و تقييم السمية الخلوية للمعقدات الفلزية المصممة بدقائق السيليكا النانوية ضد خطوط خلايا سرطان الثدي

علياء جبار احمد[1]، محاسن فيصل الياس[2]

[1]وزارة التعليم العالي و البحث العلمي، بغداد، العراق.
[2]قسم الكيمياء، كلية العلوم للبنات، جامعة بغداد، بغداد، العراق.

الخلاصة

في هذا البحث تم تحضير المركبات الفلزية الجديدة لأيونات البلاتين (الرباعي) و الذهب (الثلاثي) مع ليكاند قاعدة مانح جديد مشتق من السيبروفلوكساسين . تم استخدام المعقدات بعد ذلك كمصدر لتحضير جزيئات SiO_2 / PtO_2 , SiO_2 / Au_2O_3 عن طريق ترسيب المعقدات على مسام دقائق السيليكا النانوية، تم تشخيص الليكاند و معقداته باستخدام أطياف الاشعة تحت الحمراء، الاشعة فوق البنفسجية ، التحليل الدقيق للعناصر، التوصيلية المولارية و درجة الانصهارمن النتائج تبين ان الصيغة العامة للمعقدات هي : $[M(L)_2Cl_2]\ nCl.H_2O$ والشكل ثماني السطوح L= n= 1,2, ليكاند قاعدة مانح M = Au(III) ,Pt(IV), , تم تشخيص التركيب الكيميائي و المورفولوجي لدقائق الاكاسيد النانوية باستخدام أطياف الاشعة تحت الحمراء، حيود الاشعة السينية ، المجهر الالكتروني الماسح ، المجهر الالكتروني النافذ و مجهر القوة الذرية. في الخطوة التالية ، تم اختبار الليكاند و معقداته و الاكاسيد النانوية كعامل مضاد للسرطان لخطوط خلايا سرطان الثدي بأستخدام تراكيز مختلفة (400،200،100،50 مايكروغرم/مل) اظهرت النتائج أن المعقدات والاكاسيد النانوية واعدة أكثر بأن تستخدم كمضادات للسرطان في المستقبل خاصة عند التراكيز العالية

الكلمات المفتاحية: السمية الخلوية ، سيبروفلوكساسين ،اكاسيد المعادن النانوية ، معقدات قاعدة مانح ، دقائق السيليكا النانوية.